



Parameterising meso-scale eddy momentum fluxes based on potential vorticity mixing and a gauge term

Carsten Eden *

IFM-GEOMAR, Theory and Modelling, Düsternbrooker Weg 20, Kiel 24105, Germany

ARTICLE INFO

Article history:

Received 14 June 2009

Received in revised form 2 October 2009

Accepted 29 October 2009

Available online 1 November 2009

Keywords:

Meso-scale eddy momentum fluxes

Potential vorticity diffusion

Friction

Parameterisation

ABSTRACT

Meso-scale fluctuations are known to drive large-scale zonal flows in the ocean, a mechanism which is currently missing in non-eddy-resolving ocean models. A closure for meso-scale eddy momentum fluxes is evaluated in a suite of idealised eddying channel models, featuring eddy-driven zonal jets. It is shown how the appearance of zonal jets, which act as mixing barriers for turbulent exchange, and reduced lateral diffusivities are linked in a natural way by implementing mixing of potential vorticity and using a gauge term to insure that no spurious forces are introduced. It appears, therefore, possible to parameterise the appearance of zonal jets and its effect on the ventilation of interior ocean basins in non-eddy-resolving, realistic ocean models.

© 2009 Elsevier Ltd. All rights reserved.

1. Introduction

It is the aim of this study to parameterise the effects of the meso-scale fluctuations forming zonal jets in an idealised model, as a first step towards an appropriate parameterisation of eddy momentum fluxes in a three-dimensional and more realistic context. Zonal jets are a well-known feature of geophysical turbulence (Rhines, 1975), can be found in all ocean basins (Treguier et al., 2003; Nakano and Hasumi, 2005; Maximenko et al., 2005; Eden, 2006) and the Southern Ocean, and it is assumed that similar jet-like structures on giant gas planets like Jupiter and the atmospheric jet stream are governed by similar dynamical mechanisms (Danilov and Gurarie, 2002; Galperin et al., 2004; Baldwin et al., 2007). The jets are formed by the lateral convergence of turbulent momentum fluxes related to meso-scale fluctuations, i.e. they are eddy-driven, and act as barriers for meridional turbulent exchange (Dritschel and McIntyre, 2008).

It is current practise in non-eddy-resolving ocean models to parameterise meso-scale eddy momentum fluxes in analogy to micro-scale processes as lateral (harmonic or biharmonic) friction, sometimes with an anisotropic viscosity tensor (Large et al., 2001). However, the existence and statistical persistence of up-gradient eddy momentum fluxes in eddy-driven jets – indicating negative turbulent viscosities – has been known, but left aside in ocean modelling, since Starr (1968). Because the zonal jets might play an important role in ventilating the interior mid-latitude ocean basins

below the thermocline (Treguier et al., 2003; Eden, 2006), a parameterisation of those features is necessary for ocean climate models predicting carbon uptake and other changes in biogeochemical cycles of the ocean.

A better mean to parameterise the effect of eddy momentum fluxes is by considering diffusion of potential vorticity – instead of momentum as in the micro-scale analogy – as first proposed by Welander (1973) and as discussed by, e.g. Marshall (1981), Killworth (1997) and Treguier et al. (1997). However, this idea is hampered by the fact that potential vorticity is not a directly predicted variable in an ocean model based on the primitive equations. As one consequence, care has to be taken in the momentum budget, such that no forces are introduced by the parameterisation which would lead to spurious integral acceleration. This goal was implemented by Wardle and Marshall (2000) and Olbers et al. (2000) in parameterisations for idealised channel models, by tuning the vertical structure of the diffusivity for the closure, while prescribing magnitude and lateral shape of the diffusivity. However, the lateral and vertical structure of the appropriate diffusivity remains unknown for the general situation in a realistic ocean model, such that it appears difficult to proceed with a prescribed diffusivity, i.e. one needs a closure for the diffusivity. A prominent example for such a closure is given by the mixing length assumption, as originally suggested for geophysical applications by Green (1970) and as recently discussed by Eden and Greatbatch (2008b).

In this study, a closure for the eddy momentum fluxes based on potential vorticity mixing and a gauge term is evaluated and tested in an idealised primitive equation model, as a first step towards the application of the closure in three-dimensional more realistic

* Tel.: +49 (0)431 600 4178.

E-mail address: ceden@ifm-geomar.de

ocean models. To construct the closure, it is assumed that the lateral diffusivity for buoyancy – appropriate to the thickness diffusivity of the Gent and McWilliams (1990) parameterisation – is identical to the one for potential vorticity. While that diffusivity is thought to be fixed by an additional closure – for instance by a mixing length assumption – the constraint on the momentum budget by the global angular momentum conservation is satisfied by introducing a rotational eddy potential vorticity flux given by a gauge term. This gauge term is set in order to satisfy the momentum constraint such that no spurious forces are introduced by the closure.

The next section will detail the closure for the eddy momentum budget for the zonally averaged case in quasi-geostrophic approximation and the application of the momentum constraint by rotational potential vorticity fluxes. Section 3 presents the analysis of a suite of eddying channel model experiments, while in Section 4 the closure is validated based on the eddying models and tested in a zonally averaged version of the model. The last section summarises and discusses the main conclusions of this study.

2. A parameterisation of eddy momentum fluxes

An idealised channel model formulated in primitive equations is analysed below, in which deviations from the zonal mean are interpreted as fluctuations associated with meso-scale eddies. The analytical treatment of the meso-scale fluctuations in the model is based on quasi-geostrophic approximation, i.e. the meso-scale dynamics are assumed to be in agreement with this approximation. The zonal mean momentum and buoyancy budgets valid within the quasi-geostrophic approximation to zero and first order are given as

$$\bar{u}_t = f\bar{v} - \bar{s}_y - r\bar{u} \quad (1)$$

$$f\bar{u} = -\left(\bar{p} + \overline{v'^2}\right)_y \quad (2)$$

$$\bar{b}_t = -\bar{w} - \bar{h}_y + \bar{Q} \quad (3)$$

where $b = b^*/N^2$ denotes buoyancy b^* divided by the stability frequency N^2 . Note that buoyancy is a perturbation with respect to a horizontally constant background buoyancy $B(z)$ with $B_z = N^2$. All variables have been expanded into zonal mean quantities (denoted by an overbar) and perturbations (denoted by primes) before taking the zonal averages, i.e. zonal velocity was expressed as $u = \bar{u} + u'$, scaled buoyancy as $b = \bar{b} + b'$, pressure as $p = \bar{p} + p'$, meridional velocity as $v = \bar{v} + v'$ and vertical velocity as $w = \bar{w} + w'$. Note that for zonal averages $\partial_x \bar{x} \equiv 0$ for any zonal mean quantity \bar{x} and that in particular the (zero order) geostrophically balanced meridional velocity vanishes by construction. Note also that the meridional momentum budget, Eq. (2), contains both the zero (geostrophic) and first (ageostrophic) order equations. $\bar{s} = \bar{u}'\bar{v}'$ denotes the meridional eddy flux of zonal momentum and $\bar{h} = v'b'$ is related to the meridional eddy buoyancy flux. An unspecified forcing function Q for buoyancy was included and linear damping with friction coefficient r for momentum to indicate micro-scale processes.

From the instantaneous Eqs. (1)–(3), a budget for the potential vorticity $q = v_x - u_y + \beta y + fb_z$ can be constructed. Taking the zonal mean of this potential vorticity budget yields

$$\bar{q}_t = -\bar{d}_y + r\bar{u}_y + f\bar{Q} \quad (4)$$

where $\bar{d} = \bar{q}'\bar{v}'$ denotes the eddy potential vorticity flux. Note that

$$\bar{d} = -\bar{s}_y + f\bar{h}_z \quad (5)$$

which relates eddy potential vorticity fluxes in the mean potential vorticity budget, Eq. (4), with eddy momentum and buoyancy fluxes. Note also that it is possible to add an arbitrary function of depth and time to the eddy potential vorticity flux, playing the role of a rotational eddy potential vorticity flux, which can always be

added since it does not contribute to the flux divergence in Eq. (4). This fact will be utilised below for the parameterisation of eddy momentum fluxes in order to satisfy a global constraint on the parameterised version of \bar{s}_y .

First proposed by Green (1970), it became a common approach to assume that the lateral eddy buoyancy flux is directed down the mean gradient, i.e. that

$$\bar{h} \approx -K\bar{b}_y \quad (6)$$

where K denotes a lateral diffusivity which has to be specified, e.g. using the closure of Eden and Greatbatch (2008b) which is detailed in Appendix A. Note that K is equivalent to the isopycnal thickness diffusivity in the Gent and McWilliams (1990) parameterisation. Note also, however, that the explicit choice (or closure) for K is not essential for the closure for the eddy momentum fluxes as discussed in this section.

To obtain the remaining closure for \bar{s} , it is assumed that for the eddy potential vorticity fluxes a similar relation as Eq. (6) holds for potential vorticity as well

$$\bar{d} \approx -K'\bar{q}_y - \bar{\theta} \quad (7)$$

Note that a rotational flux component was added to the eddy potential vorticity flux (or, equivalently, to Eq. (5) relating the eddy fluxes of potential vorticity with buoyancy and momentum fluxes) given by $\bar{\theta}(z, t)$, which drops out taking the meridional divergence of the eddy potential vorticity flux in the mean potential vorticity budget. $\bar{\theta}$ will be specified below to satisfy a constraint on the parameterised zonal momentum budget. From the relation Eq. (5) and using the downgradient closures Eqs. (6) and (7), an expression for the eddy forcing \bar{s}_y in the mean zonal momentum budget can then be derived

$$\bar{s}_y = -K'(\bar{u}_{yy} - \beta) - K_z f \bar{b}_y - \frac{f^2}{N^2} (K' - K) \bar{u}_{zz} + \bar{\theta} \quad (8)$$

Note that for simplicity, it will be assumed below that eddy potential vorticity and buoyancy fluxes share the same diffusivity; i.e. $K' = K$, an assumption which is validated in detail in the numerical experiments. Using expression Eq. (8), the mean momentum budget, Eq. (1), becomes

$$\bar{u}_t = f\bar{v} + K'(\bar{u}_{yy} - \beta) + K_z f \bar{b}_y + \frac{f^2}{N^2} (K' - K) \bar{u}_{zz} - \bar{\theta} - r\bar{u} \quad (9)$$

Note that the first term of the parameterised version of \bar{s}_y , i.e. $K'\bar{u}_{yy}$ in Eq. (8) acts akin (but not identical) to lateral friction and is related to the meridional gradient of relative vorticity. Further, a difference between the diffusivities for buoyancy and potential vorticity in Eq. (8) is akin to vertical friction with diffusivity $f^2/N^2(K' - K)$ (note that here $f\bar{b}_{yz} \approx -f^2/N^2\bar{u}_{zz}$ was assumed). The other components of the parameterised version have a different form than friction. In particular, the term $K'\beta$ introduces a westward force, already suggesting the need for a compensating eastward force, which will in fact be given by the gauge term $\bar{\theta}$.

The closure given by Eq. (8) was originally proposed in similar form by, e.g. Welander (1973), Marshall (1981), Killworth (1997) and Treguier et al. (1997). It was noted in the later studies that any closure for the eddy momentum fluxes also have to take care of the global zonal momentum constraint (Bretherton, 1966), i.e. it has to be insured that

$$0 = - \int_{-h}^0 \int_0^L \bar{s}_y dy dz \\ = \int_{-h}^0 \int_0^L \left(K'(\bar{u}_{yy} - \beta) + K_z f \bar{b}_y + \frac{f^2}{N^2} (K' - K) \bar{u}_{zz} - \bar{\theta} \right) dy dz. \quad (10)$$

Note that the integral over the eddy momentum flux vanishes because of the boundary conditions for the flux. In principle, the con-

straint Eq. (10) holds for any parameterisation for eddy momentum fluxes, i.e. also when using lateral friction corresponding to the micro-scale analogue, which is, however, usually ignored. The numerical experiments, on the other hand, will demonstrate the need to obey the constraint for a parameterisation of eddy momentum fluxes based on potential vorticity mixing. While in Wardle and Marshall (2000) and Olbers et al. (2000) the constraint was satisfied by the choice of K , in this study it is satisfied by the choice of the gauge term θ , as detailed below.

The choice $K = K'$ simplifies the system, since one has to supply a closure for one K only, which could for instance be given by the closure of Eden and Greatbatch (2008b) based on the mixing length assumption of Green (1970). However, it should be noted that there are also hints that both K 's can be different (Smith and Marshall, 2009). Note also that when isopycnals and isolines of mean potential vorticity are rather different, diffusion along isopycnals, not felt by the buoyancy, might be related to a difference between the diffusivities. In other words, potential vorticity is mixed also by isopycnal diffusion as a passive tracer with a gradient on mean isopycnals, and is not just advected by the bolus velocity like buoyancy. However, it will be shown below that the numerical experiments support the assumption of identical diffusivities for potential vorticity and buoyancy.

3. An idealised eddying channel model

3.1. Setup of the numerical experiments

The closure discussed in Section 2 is evaluated in a primitive equation model in Cartesian coordinates on a β -plane. The numerical code of the model can be found at <http://www.ifm-geomar.de/~cpflame>. The model is configured as a channel forced at the side walls by restoring zones. These zones are 6 grid points wide, located at the northern and southern boundary and relax the buoyancy towards the initial condition for b^* , which is characterised by a state with specified linear meridional ($b_y^* \equiv M_0^2$) and vertical ($b_z^* + B_z \equiv N_0^2$) gradients and no zonal variations. Note that the actual simulated zonally averaged buoyancy deviates not very much from the initial state, despite strong eddy activity. Dissipation

($\mathcal{R}_u, \mathcal{R}_v$) is given by biharmonic diffusion and friction and additionally by an interior linear drag with coefficient r . The quadratic channel of width $L = 4000$ km is resolved by 256×256 grid points and is 2000 m deep with 40 levels. The horizontal (vertical) resolution is constant at approx. 16 km (50 m). Boundary conditions are free slip and zero buoyancy fluxes at top, bottom and lateral boundaries. The biharmonic mixing and interior drag represents the unresolved effects of dissipation by smaller scale dynamics on the quasi-geostrophic dynamics in the model, while the restoring near the side walls represents large-scale baroclinic forcing of the flow.

The setup is characterised by a basin Rossby number $Ro = \frac{M_0^2 h}{f^2 L}$, Burger number $Bu = \frac{N_0^2 h^2}{f^2 L^2}$ and an Ekman number $Ek = \frac{r}{f}$ related to the interior drag. Resulting important parameters are the Rossby radius $L_r = \frac{N_0 h}{f \pi}$ and the inverse Eady growth rate $\sigma = \frac{N_0}{M_0^2}$. Fig. 1 shows a snapshot of velocity and buoyancy at 500 m depth in an experiment with $L_r = 96$ km and $\sigma = 4.8$ d. All values of these variables which has been used in the numerical experiments are listed in Table 1. In all experiments only N_0^2 and M_0^2 of the target buoyancy in the restoring zones were modified, while all other model parameters were held fixed (except for the drag coefficient, see below). Note that the constant meridional buoyancy gradient M_0^2 is positive if not explicitly stated but in some experiments taken to be negative. Note also that for the experiments with largest Eady growth rates ($\sigma = 3.2$ d) the drag coefficient was increased from $r = (116\text{d})^{-1}$ to $r = (29\text{d})^{-1}$ to obtain a stable integration.

3.2. Global energy cycle in the experiments

In order to describe the individual experiments with meaningful integral numbers, the domain averaged energy cycle in the various experiments is presented in Table 1. Note that the energy cycle, given by the budgets for eddy and mean kinetic energy (EKE and MKE, respectively) and the eddy and mean potential energy (EPE and MPE, respectively), together with the dissipative terms and exchange terms between the budgets, is defined in detail in Appendix B. All values have been averaged over 4 years fol-

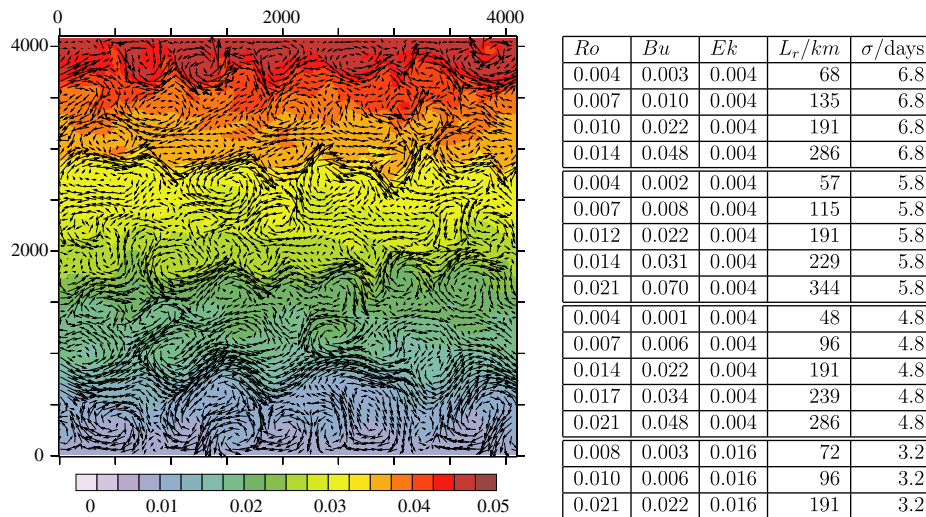


Fig. 1. (Left) Snapshot of velocity and (full, unscaled) buoyancy in m/s^3 in an experiment with Rossby radius $L_r = 96$ km and inverse Eady growth rate $\sigma = 4.8$ d at $z = -500$ m after 600 days of integration. Zonal and meridional axis are in km. Right) Basin Rossby number ($Ro = \frac{M_0^2 h}{f^2 L}$) basin Burger number ($Bu = \frac{N_0^2 h^2}{f^2 L^2}$) basin Ekman number ($Ek = \frac{r}{f}$) first baroclinic Rossby radius ($L_r = \frac{Nh}{rf}$) and inverse Eady growth rate ($\sigma = \frac{N}{M^2}$) for the different numerical experiments. While channel depth (h), width (L) and Coriolis parameter (f) where held fixed, the vertical (N^2) and lateral (M^2) buoyancy gradient and, when necessary, the interior drag coefficient (r) were varied in the experiments.

Table 1

Long term and basin integrated zonal mean energies in $10^9 \text{ m}^4/\text{s}^2$ in the experiments characterised by Rossby radius L_r and inverse Eady growth rate σ . Arrows denotes energy transfer terms in m^4/s^3 and are positive in the direction they point to. The last three experiments have a reversed prescribed mean meridional buoyancy gradient.

L_r/km	σ/d	MKE	→	MPE	→	EPE	→	EKE	→ MKE
68	6.8	0.02	-1.70	15.0	18.5	0.05	13.0	0.04	1.8
135	6.8	0.06	-6.45	15.2	31.6	0.08	26.4	0.09	5.4
191	6.8	0.09	-12.6	15.3	42.0	0.12	36.2	0.13	6.7
286	6.8	0.16	-26.5	15.8	50.3	0.12	44.1	0.17	5.4
57	5.8	0.03	-1.83	21.0	36.0	0.10	24.3	0.07	3.6
115	5.8	0.09	-6.58	21.1	58.1	0.14	48.7	0.15	11.8
191	5.8	0.16	-17.0	21.0	75.8	0.18	67.0	0.23	14.4
229	5.8	0.18	-24.0	20.8	85.0	0.21	76.5	0.29	11.9
344	5.8	0.31	-49.1	21.6	93.0	0.22	84.3	0.31	13.5
48	4.8	0.04	-1.96	31.1	62.2	0.18	38.3	0.10	6.6
96	4.8	0.14	-6.70	30.6	108	0.27	88.6	0.26	23.0
191	4.8	0.31	-23.4	30.6	142	0.29	129	0.39	38.6
239	4.8	0.35	-39.5	30.4	153	0.33	140	0.50	31.0
286	4.8	0.40	-52.9	30.3	166	0.37	154	0.56	28.8
72	3.2	0.05	-34.6	75.2	217	0.53	153	0.16	2.5
96	3.2	0.08	-58.1	79.2	273	0.65	212	0.23	4.3
191	3.2	0.26	-195	73.8	424	0.72	390	0.45	14.9
135	6.8	0.05	-6.6	14.9	33.6	0.09	28.0	0.10	3.1
96	4.8	0.12	-7.2	30.7	109	0.28	89.0	0.29	17.4
96	3.2	0.07	-57.9	77.5	276	0.64	216	0.24	2.9

lowing the spin-up period of each experiment. MPE dominates as the largest energy reservoir in all experiments and is given by the effect of the restoring zones at the side walls of the channel, i.e. MPE is proportional to the inverse Eady growth rate σ implied by the restoring zones in the experiments. EKE and EPE are similar in size and the ratio of EPE to EKE becomes smaller (larger) than one going to larger (smaller) Rossby radii L_r . For constant L_r the ratio of EPE to EKE increases with increasing σ . The MKE is of similar magnitude as EKE but never exceeds the level of EKE. The ratio of MKE to EKE increases with L_r , but appears to stay constant with σ .

Also shown in Table 1 are the energy transfer terms between the different energy forms, while Table 2 shows the dissipative energy transfers. In all experiments, there is large production of MPE related to the effect of the restoring zones. MPE production increases with L_r and Eady growth rates σ^{-1} . The MPE is transferred to EPE and to a smaller amount to MKE. The EPE is to a smaller

amount dissipated by the biharmonic mixing (the restoring has only a weak effect on EPE) but to a larger amount transferred to EKE related to the effect of baroclinic instability. In the EKE budget the largest amount of dissipation is found, while a smaller amount of EKE is transferred to MKE, related to the effect of barotropic instability. Note that this energy transfer rectifies the mean flow. For the dissipation of kinetic energy, the interior drag was found to be more important than the biharmonic friction in all experiments.

While the reservoirs of the energy differ between the experiments, the sign of the energy transfers remains the same in each experiment. In particular, there is always transfer of EKE to MKE, i.e. eddy driven mean flow in all experiments. This energy transfer appears to increase with increasing Eady growth rate σ^{-1} , although the experiments with largest Eady growth rates show less energy transfer of EKE to MKE, but note that here the interior drag was also modified. Note also that the sign of the meridional buoyancy gradient, M^2 , does not effect the energy levels, transfers and dissipation rates.

Table 2

Dissipation of EKE and EPE by interior drag ($r|\bar{u}'|^2$), horizontal biharmonic friction ($\epsilon_{biha} = |\nabla \cdot A_{biha} \nabla u'|^2$) and mixing ($\bar{b}'\bar{Q}' = |\nabla \cdot A_{biha} \nabla b'|^2$) and restoring and dissipation of MKE (by drag and biharmonic friction) and MPE (by mixing and restoring zone) in m^4/s^3 for the individual experiments characterised by L_r and σ . The last three experiments have a reversed prescribed mean meridional buoyancy gradient.

L_r/km	σ/d	ϵ_{biha}	$r \bar{u}' ^2$	$\bar{b}'\bar{Q}'$	rest.	MKE diss.	MPE diss.
68	6.8	3.6	7.8	5.0	0.6	3.5	-20
135	6.8	3.6	17.6	4.0	1.2	11.8	-37
191	6.8	3.7	25.6	4.0	1.8	19.3	-49
286	6.8	4.3	33.6	3.9	2.3	31.9	-56
57	5.8	7.1	13.7	10.4	1.4	5.4	-40
115	5.8	7.4	29.8	7.4	2.0	18.4	-70
191	5.8	7.2	45.6	5.8	3.1	31.4	-90
229	5.8	7.5	58.0	5.6	3.0	36.0	-97
344	5.8	8.5	62.5	5.0	3.7	62.6	-106
48	4.8	11.8	20.7	20.6	3.3	8.5	-69
96	4.8	14.9	52.0	14.9	4.6	29.7	-131
191	4.8	12.1	79.2	8.2	4.4	62.0	-180
239	4.8	11.2	100	7.5	5.1	70.6	-184
286	4.8	13.5	112	7.1	5.5	81.7	-195
72	3.2	21.3	130	48.8	15.2	37.2	-219
96	3.2	19.7	188	40.0	20.9	62.4	-277
191	3.2	16.3	359	18.2	15.1	210	-439
135	6.8	3.9	20.9	4.3	1.3	9.7	-37
96	4.8	15.4	57.4	15.0	5.4	24.6	-127
96	3.2	20.8	193	40.3	19.2	60.8	-279

3.3. Eddy-driven jets in the experiments

Fig. 2 shows the zonally averaged (time mean) zonal velocity and buoyancy and Fig. 3 the EKE and also the EKE production terms $N^2 b' w' - \bar{s}\bar{u}_y$ for several different choices of L_r and σ . In the experiment with $L_r = 96 \text{ km}$ and $\sigma = 4.8 d$ four eastward zonal jets develop which can be already seen in the snapshot in Fig. 1. The jets are surface intensified while near the bottom, weak westward flow is found. The eddy activity is also surface intensified while near the bottom only weak eddy activity is found. Transfer from EPE related to baroclinic instability ($N^2 b' w'$) dominates below 500 m depth the production of EKE with slight maxima within and below the jets. In the upper layer, however, barotropic instability ($-\bar{s}\bar{u}_y$) gets larger, but with opposite sign, such that there is energy transfer from EKE to MKE driving the zonal jets. In the other experiments similar jets show up, with a tendency for larger meridional scale for larger levels of EKE. However, for the experiments with $\sigma = 3.2 d$, the experiments with highest energy production by baroclinic instability (largest Eady growth rates), a significant zonal jet structure can only be found for the largest Rossby radius.

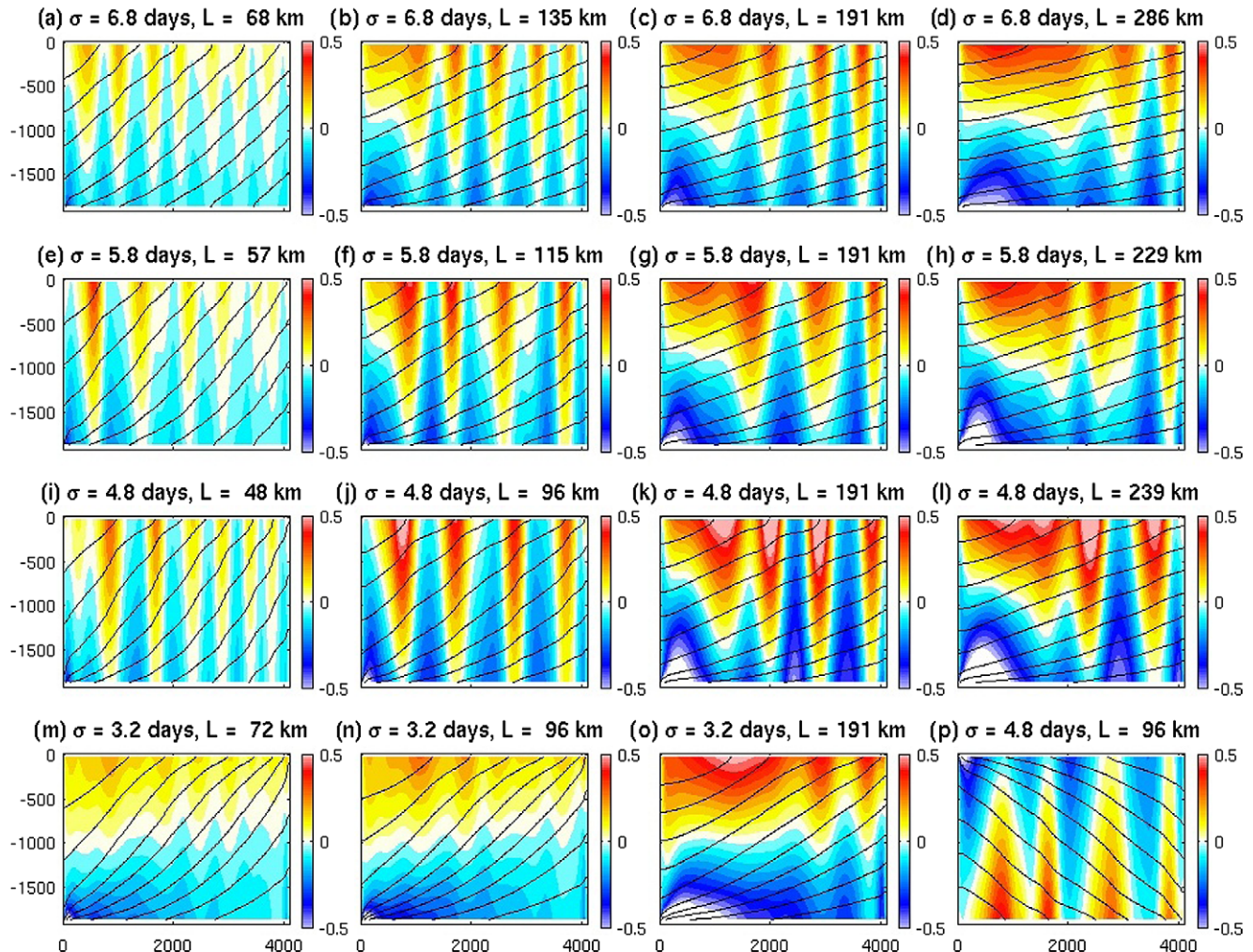


Fig. 2. Zonal mean zonal velocity in m/s in the different experiments. The vertical axis denotes depth in m and the horizontal axis latitude in km. Also shown are mean isopycnals (solid lines). The basin-wide inverse Eady growth rate σ and Rossby radius L taken from Table 1 for the corresponding experiments are indicated in the figures. For (case p), the meridional buoyancy gradient was reversed.

Reversing the meridional buoyancy gradient (M^2), the simulations are almost identical with respect to the integral energy levels and transfers, but vertically reversed in some aspects. It is clear that the vertical shear of \bar{u} reverses by construction in those experiments. However, bottom intensified EKE and in consequence, bottom intensified eddy-driven, eastward zonal jets are found for $\bar{b}_y < 0$ and near the surface weak westward flow as seen in Figs. 2p and 3p. The dependency of the intensification of the jets on the sign of M^2 may come as a surprise, but note that no other process (such as bottom friction or surface wind stress) favors bottom or surface intensification in the model setup. Note also that regardless of the sign of M^2 , eastward jets and only weak westward flow shows up.

same combinations of prescribed Rossby radius L , and inverse Eady growth rate σ as in Fig. 2.

Magnitudes of both diffusivities vary within the model domain and also amongst all experiments from zero to more than 20000 m²/s. At some places both diffusivities get negative, but regions with positive diffusivities dominate in each case. Within the eastward surface jets, both diffusivities are significantly reduced, indicating barriers for turbulent exchange, i.e. mixing barriers, across the zonal jets (Dritschel and McIntyre, 2008).

Despite the large variations within the model domain and amongst the experiments, both diffusivities are indeed rather similar in the individual experiments, with respect to magnitude and spatial pattern. Note that this is despite very different mean fields of potential vorticity and buoyancy (and eddy fluxes, not shown). In particular, the minima within eastward jets are seen in both diffusivities in all experiments. The vertical structure with large values near the bottom and smaller values near the surface are also similar in all experiments and visible in both diffusivities. Note that reversing the meridional buoyancy gradient (M^2) the vertical structure of K and K' also reverses, as seen before for EKE and energy exchange terms. Note also that in many cases, \bar{q}_y shows a zero crossing at mid-depth, for which the estimated diffusivity K' has a singularity with the effect of large values of fluctuating sign in the vicinity of the zero crossing (while there is no such zero crossing for \bar{b}_y).

4. Testing the meso-scale eddy closure

4.1. Validation of the closure in the eddying model

An important assumption of the closure for the eddy momentum fluxes is given the assumption of identical diffusivities for eddy potential vorticity and buoyancy fluxes, i.e. $K = K'$ in Eqs. (8)–(10). Fig. 4 and Fig. 5 shows the diffusivities estimated from the flux-gradient relationship $\bar{h} = -K\bar{b}_y$ and $\bar{d} = -K'\bar{q}_y$, for the

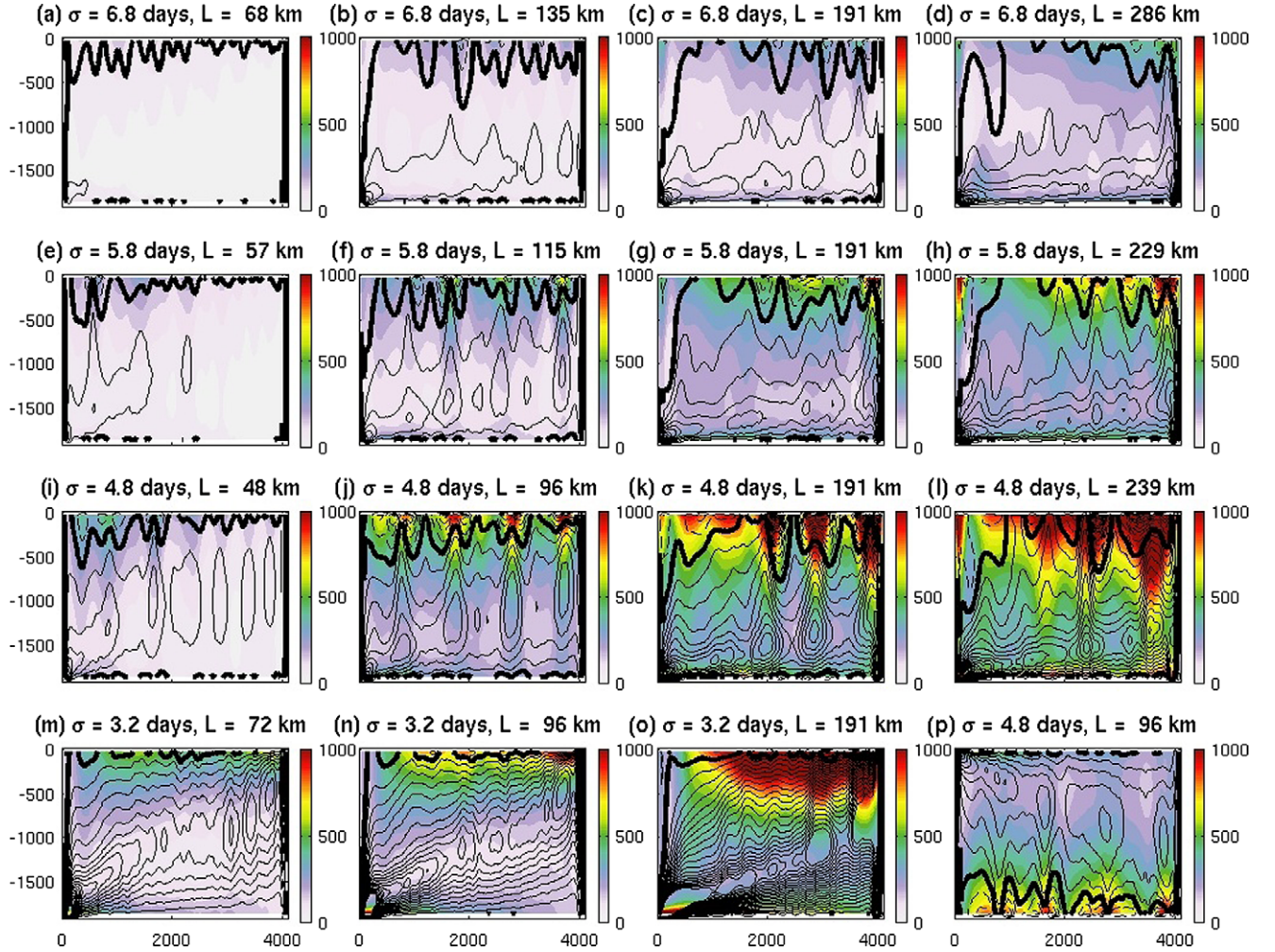


Fig. 3. Zonal mean EKE in cm^2/s^2 and EKE production term (lines, $10^{-9} \text{ m}^2/\text{s}^3$, contour spacing is $5 \times 10^{-9} \text{ m}^2/\text{s}^3$, positive (negative) values correspond to solid (dashed) lines and denote production (removal) of EKE in the different experiments. The basin-wide inverse Eady growth rate σ and Rossby radius L taken from Table 1 for the corresponding experiments are indicated in the figures. For (case p), the meridional buoyancy gradient was reversed.

Near the zero crossing of \bar{q}_y , differences between both diffusivities are largest in all experiments. Note that this region corresponds to the depth level at which the first baroclinic Rossby wave speed Doppler shifted by the mean flow cancels, i.e. to the steering level of unstable Rossby waves, where mixing is believed to be most intense (Green, 1970; Smith and Marshall, 2009). Correspondingly, both diffusivities show maxima near the steering level, but K' becomes ill-defined because of the change of sign in \bar{q}_y and rather different to K . Note that in some experiments, near surface values of K' tend to be larger than the corresponding diffusivity for buoyancy. On the other hand, in the interior both diffusivities are similar, such that it is concluded here that the assumption of identical diffusivities for buoyancy and potential vorticity ($K = K'$) appear valid for this model setup. Note that this assumption will be further tested below by evaluating the performance of the closure.

4.2. Validation in a zonally averaged model version

In this section, the closure for the eddy momentum fluxes is applied to a zonally averaged numerical model, which is discretised on the same meridional, vertical and temporal grid as the eddying channel model, and with identical subgrid-scale parameterisations and forcing Q , \mathcal{R}_u and \mathcal{R}_v (biharmonic friction and diffusion, a lin-

ear drag in the momentum budget relaxation zones for buoyancy near the side walls of the channel) using the identical numerical code (whenever possible).

As noted above, the dynamics of the meso-scale eddies are assumed to be described within the quasi-geostrophic approximation. For the large-scale mean-flow, however, this is not the case and the closure has to be implemented in the full primitive equations. The budget for the zonally averaged (unscaled) buoyancy \bar{b}^* is given by

$$\bar{b}_t^* + v^* \bar{b}_y^* + w^* (\bar{b}_z^* + N^2) = N^2 \bar{Q} \quad (11)$$

using the residual mean meridional and vertical velocity v^* and w^* given by $v^* = \bar{v} + \Psi_z$ and $w^* = \bar{w} - \Psi_y$ with the streamfunction for the eddy-driven flow, $\Psi = K \bar{b}_y^*/(\bar{b}_z^* + N^2)$, for which the parameterisation Eq. (6) has been used. It was also assumed that eddy fluxes are directed along isopycnals, i.e. any diapycnal mixing by meso-scale eddies was ignored (see Eden and Greatbatch (2008a) for a discussion of this effect). Note that the concept of the residual mean theory which is adopted here, is for instance described in Andrews et al. (1987), McDougall and McIntosh (1996) or Eden et al. (2007). Note also that within quasi-geostrophic approximation and using the parameterisation Eqs. (6), (11) simplifies to Eq. (3).

The residual mean buoyancy budget is supplemented by the mean momentum budget, either in the familiar Eulerian mean

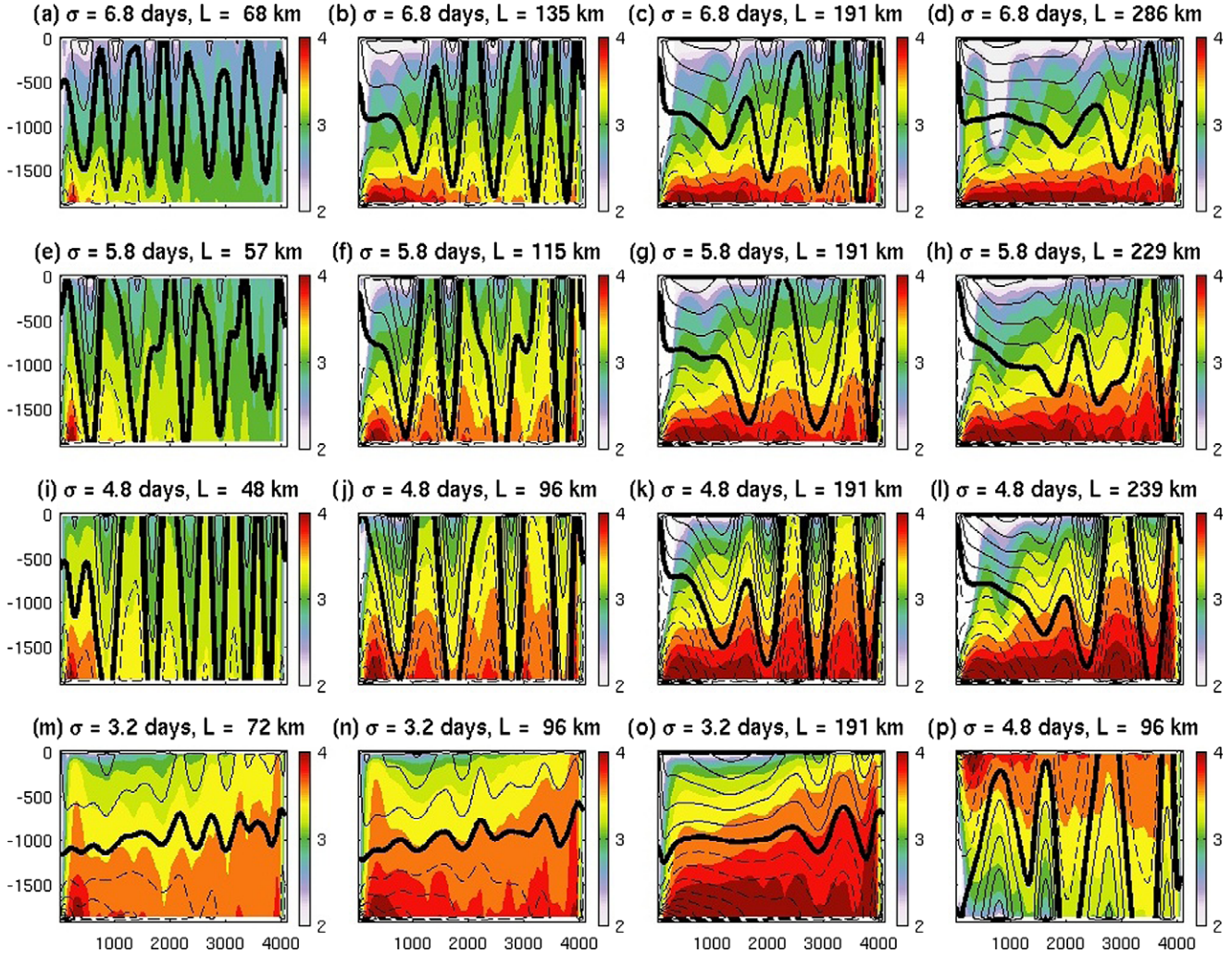


Fig. 4. Lateral diffusivity K estimated from Eq. (6), i.e. from the meridional eddy buoyancy flux and mean buoyancy in $\log_{10}(K/\text{m}^2/\text{s})$ in the different experiments. Also shown is \bar{u} (contour lines). For (case p), the meridional buoyancy gradient was reversed.

form (which is not repeated here) or, alternatively, it is possible to formulate the residual mean momentum budget

$$\begin{aligned} \bar{u}_t + v^* \bar{u}_y + w^* \bar{u}_z &= f \bar{v}^* + K(\bar{u}_y - f)_y + K(f^2 N^{-2} \bar{u}_z)_z - \bar{\theta} - \mathcal{R}_u(\bar{u}) + \delta_u \\ v_t^* + v^* v_y^* + w^* v_z^* &= -f \bar{u} - (\bar{p} + \bar{e})_y - \mathcal{R}_v(\bar{v}^*) + \delta_v \end{aligned} \quad (12)$$

using the closure Eq. (8) for the (lateral) eddy momentum fluxes (with $K = K'$), assuming $\overline{v^2} \approx \bar{e}$ and neglecting vertical eddy momentum fluxes consistent with the local quasi-geostrophic approximation. \mathcal{R}_u and \mathcal{R}_v denotes small-scale dissipation acting on the zonal and meridional momentum, respectively.

An ocean model can be based on both formulations (Ferreira and Marshall, 2006; Zhao and Vallis, 2008): Using the familiar Eulerian mean form, the Eulerian mean velocities \bar{v} and \bar{w} are given and in the buoyancy budget Eq. (11), additional eddy advection (bolus) velocities given by Ψ are added to \bar{v} and \bar{w} in order to obtain v^* and w^* . Using Eq. (12) on the other hand, the calculation of bolus velocities is not necessary since the residual mean velocities v^* and w^* are already given. Note, however, that in Eq. (12), several terms combined in $\delta_u = \Psi_z \bar{u}_y - \Psi_y \bar{u}_z$ and $\delta_v = \Psi_{zt} + r\Psi_z + \Psi_z \bar{v}_y - \Psi_y \bar{v}_z + \mathcal{R}_v(\Psi_y)$, have to be neglected in Eq. (12) in a model based on the residual mean formulation, which should both be small within the quasi-geostrophic approximation (Plumb and Ferrari, 2005). Note also that to satisfy the global momentum conservation constraint, Eq. (10), the gauge term θ can be identical for Eulerian

mean and residual mean formulation, since $\int_{-h}^0 (Kf^2/N^2 u_z)_z dz = 0$ for free slip vertical boundary conditions for \bar{u} .

The equivalence of the Eulerian and the residual mean formulation was tested for the present model setup, neglecting for the moment any parameterisation for the eddy momentum fluxes \bar{s} , i.e. the terms $-\bar{s}_y = K(u_y - f)_y - K_z f^2 N^{-2} \bar{u}_z - \theta$ are set to zero in the Eulerian or residual mean momentum budget, such that the zonal residual momentum equation, Eq. (12), becomes

$$\bar{u}_t + v^* \bar{u}_y + w^* \bar{u}_z = f \bar{v}^* + (Kf^2 N^{-2} \bar{u}_z)_z - \mathcal{R}_u(\bar{u}) \quad (13)$$

As expected, only very small differences in all mean variables for various prescribed values of K, L_r and σ are found between the Eulerian mean model formulation (using bolus velocities in the buoyancy budget Eq. (11)) and the residual mean formulation. In the following the residual mean formulation is described only, but note that results are very similar in the alternative formulation using the bolus velocities.

4.2.1. Effect of a constant diffusivity

Fig. 6 shows the zonal mean flow in the zonally averaged model using a constant diffusivity $K = 5000 \text{ m}^2/\text{s}$ and setting $\bar{s}_y = 0$, i.e. using Eq. (13) in the zonally averaged model. Also shown in Fig. 6 is \bar{u} in the eddying channel for $L_r = 96 \text{ km}$ and $\sigma = 4.8 \text{ d}$ (which was also chosen for the zonally integrated model). The mean zonal flow in both models is clearly very different, i.e. there

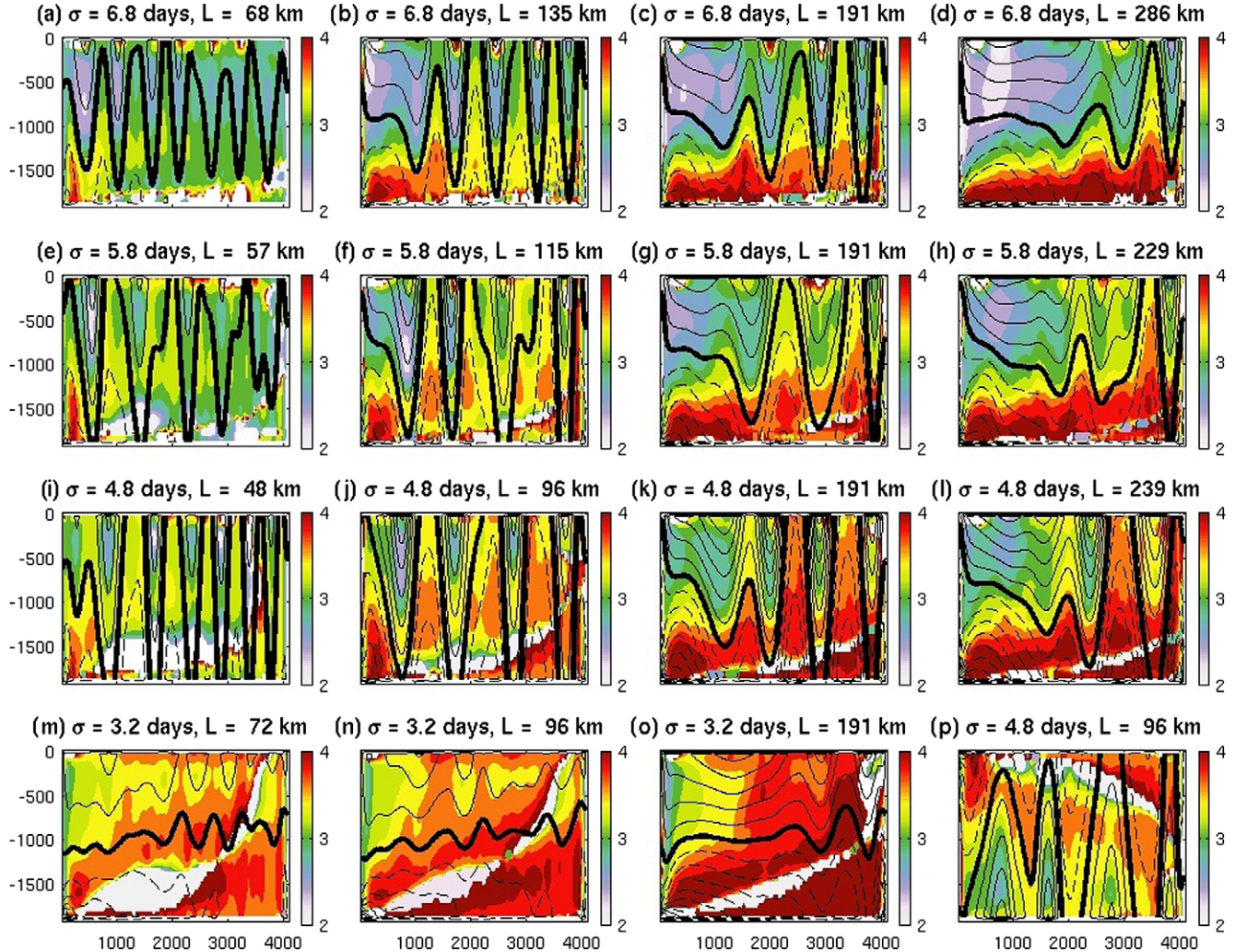


Fig. 5. Lateral diffusivity K' estimated from the meridional eddy potential vorticity flux and mean (Ertel) potential vorticity in $\log_{10}(K'/[\text{m}^2/\text{s}])$ in the different experiments (setting the rotational flux $\theta = 0$). Also shown is \bar{u} (contour lines). For (case p), the meridional buoyancy gradient was reversed.

is almost no barotropic mean zonal flow in the zonally averaged model in contrast to the eddying counterpart, featuring the energetic zonal jets.

The results do not change significantly (not shown), using the closure for \bar{s} , i.e. using Eq. (12) instead of Eq. (13) in the zonally averaged model, but still a constant diffusivity $K = 5000 \text{ m}^2/\text{s}$. However, now, using the closure for \bar{s} , the gauge term θ has to be set to satisfy the global momentum constraint, i.e.

$$\theta = \frac{1}{Lh} \int_0^L \int_{-h}^0 \mathcal{F}_u dz dy \quad (14)$$

with $\mathcal{F}_u = K(\bar{u}_{yy} - \beta)$ and where L denotes the channel width and h its depth. Although the closure with a constant diffusivity has not a large effect, it is important to note that the gauge term θ is mandatory to balance the term $K\beta$ in Eq. (12) (the term $K\bar{u}_{yy}$ is much smaller in the experiment with constant K) which would otherwise lead to an artificial strong westward acceleration of the zonal mean flow (not shown). This demonstrates the need for satisfying the global momentum constraint of Bretherton (1966) for a parameterisation of eddy momentum fluxes.

4.2.2. Effect of horizontal variations in K

Allowing for a horizontal structure in K , the mean zonal flow of the zonally averaged model changes significantly: Fig. 7 shows \bar{u}

for a case with horizontal variations of K , i.e. for $K = 5000(1 + 0.1 \sin(8\pi y/L)) \text{ m}^2/\text{s}$. For a model integration without the closure, i.e. setting $\bar{s} = 0$ and using Eq. (13), the zonal mean flow is close to geostrophic balance with a very weak barotropic component as shown in Fig. 7a). The small-scale sinusoidal horizontal variations in \bar{u} in that experiment are only caused by corresponding small-scale sinusoidal variations in \bar{b}_y , which are in turn caused by corresponding variations in the streamfunction for the eddy driven advection, Ψ . On the other hand, Fig. 7b) shows that a strong barotropic component develops in the zonally averaged model, when adding the parameterisation $K(u_{yy} - \beta) - \theta$ to the zonal momentum budget, i.e. using Eq. (12) instead of Eq. (13), with the gauge term θ set as in Eq. (14) with $\mathcal{F}_u = K(\bar{u}_{yy} - \beta)$.

Eastward jets can be found for local minima of K , while maxima correspond to westward barotropic flow. This is consistent with the eddying model, where K show indeed also local minima within eastward jets. The response of the model to the horizontal variations in K can be understood by the adjustment of \bar{u} to the meridional variations in the forcing $K\beta$: It is only the meridional mean of $K\beta$ which can be balanced by the gauge term θ , such that the meridional variations in $K\beta$ given by the variations in K cause locally a force of alternating sign in the momentum budget. This force is balanced predominantly by the term $K\bar{u}_{yy}$ (while the interior friction remains small), i.e. the zonal flow develops the corresponding curvature in \bar{u} to balance the effect of the horizontal

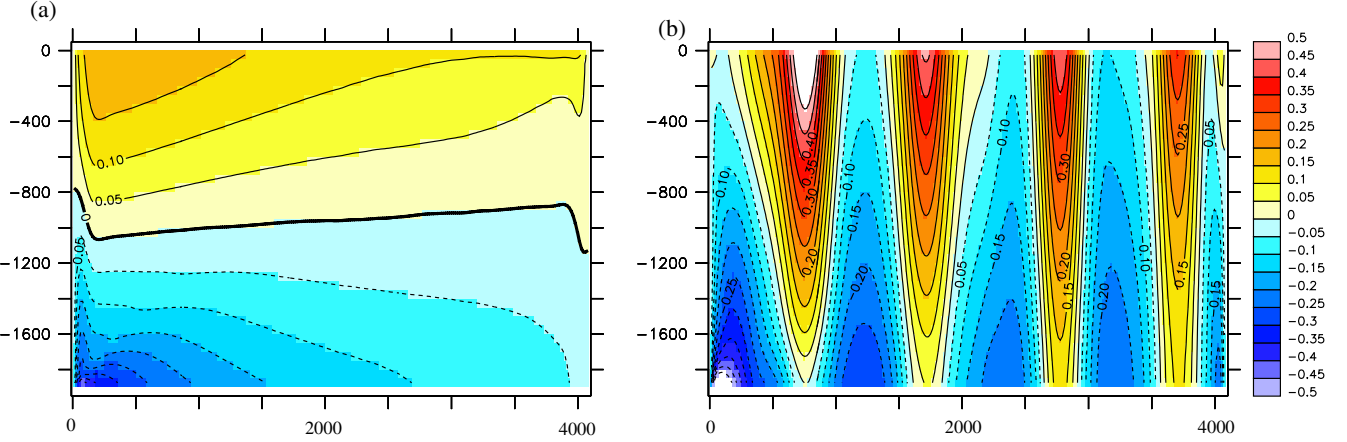


Fig. 6. Zonal mean zonal flow in m/s in coarse resolution model (a) and eddying model (b) both for $L_r = 96$ km and $\sigma = 4.8$ d. For the coarse model a constant thickness diffusivity of 5000 m²/s was used and no parameterisation for the eddy momentum fluxes.

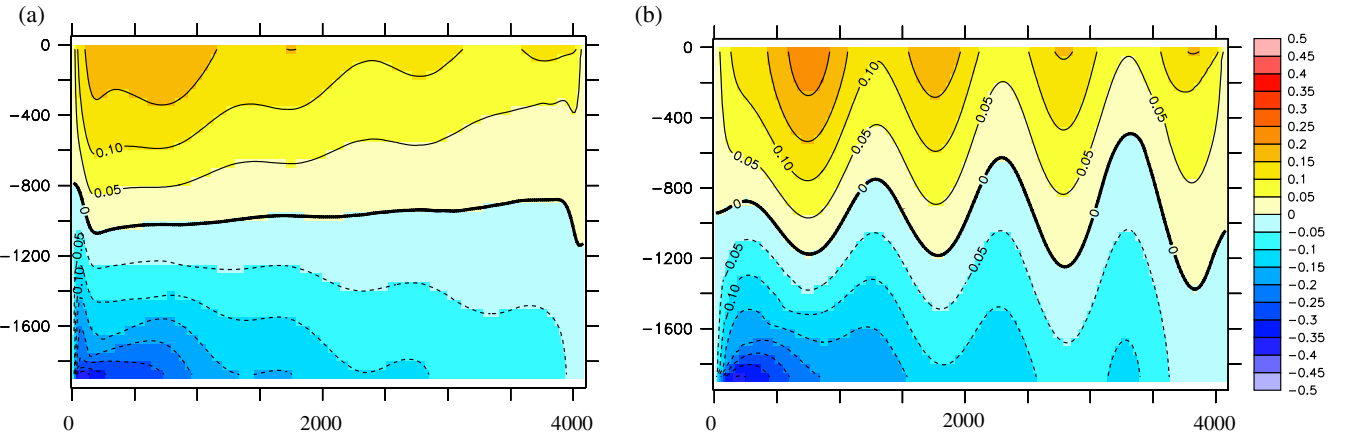


Fig. 7. Zonal mean zonal flow in m/s in the coarse resolution model for $K = 5000(1 + 0.1 \sin(y/\pi/8))$ m²/s without (a) and with (b) parameterisation of eddy momentum fluxes both for $L_r = 96$ km and $\sigma = 4.8$ d.

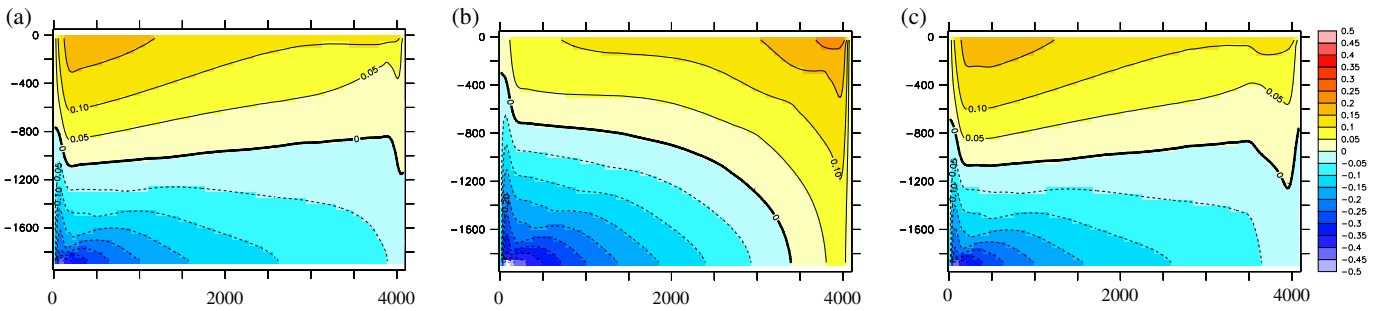


Fig. 8. Zonal mean zonal flow in m/s in the coarse resolution model for $K = 5000(1 + 0.2|z|/h)$ m²/s without (a) and with a parameterisation of eddy momentum fluxes and $\theta = 1/V \int F_u dz$ (b) and $\theta = 1/V \int F_u dz$ where the integral is taken over a sub-domain of the channel (c).

variations in $K\beta$. This curvature in \bar{u} forms the zonal jets, and is therefore a consequence of meridional variations in K and the implementation of mixing of potential vorticity.

4.2.3. Effect of vertical variations in K

Fig. 8a) shows \bar{u} for a case with $K = 5000(1 + 0.2|z|/h)$ m²/s in a model integration with $\bar{s}_y = 0$, i.e. using Eq. (13), while Fig. 8 b) shows \bar{u} for a simulation using the closure for \bar{s} , i.e. using Eq. (12) instead of Eq. (13), with the gauge term θ set as in Eq. (14) with $F_u = K(u_{yy} - \beta) - Kf^2N^{-2}\bar{u}_z$. Note that the term $K(\bar{u}_{yy} - \beta)$

in the zonal momentum budget, Eq. (13), does not affect the results much because no horizontal variations in K have been prescribed. In case of K increasing with depth a surface (bottom) intensified eastward (westward) flow can be found in the northern (southern) part of the domain, while the opposite can be found for K decreasing with depth.

Such a strong and basin-wide meridional shear in the barotropic component of \bar{u} (Fig. 8b) have not been observed in the eddying experiments (Fig. 2), although much stronger vertical variations in K have been estimated (Fig. 5) as prescribed in the zonally

averaged model. The effect can be attributed to a conflict with quasi-geostrophic scaling: For a narrow channel within quasi-geostrophic approximation, the constant gauge θ could entirely balance the term $K_z f^2 N^{-2} \bar{u}_z \approx -K_z f_0 M_0^2 / N_0^2$ in the zonal momentum budget, such that no force on the zonal flow would be generated. In the wide channel model, however, the Coriolis parameter $f = f_0 + \beta y$ is substantially changing (from 0.25 to $1.8 \times 10^{-4} \text{ s}^{-1}$) and the term $K_z f^2 N^{-2} \bar{u}_z$ shows therefore, a strong increase towards the north (variations due to the term $N^{-2} \bar{u}_z$ are of minor importance), generating a force which locally cannot be completely balanced by the constant gauge term θ . In consequence, the interior friction, $-r\bar{u}$, balances the residual local force in the zonal momentum budget, $K_z f^2 N^{-2} \bar{u}_z - \theta$, to a large extent (the term $K\bar{u}_{yy}$ remains small). Thus, the large change of f cause the strong meridional shear in the barotropic component of \bar{u} . On the other hand, the term $K_z f^2 N^{-2} \bar{u}_z$ would become $K_z f_0^2 N_0^{-2} \bar{u}_z$ within quasi-geostrophic approximation, and could be locally balanced by the constant gauge term θ and would thus show much weaker meridional variations, with no large effects on \bar{u} .

When allowing for a small meridional dependency of θ , the basin-wide meridional shear in \bar{u} vanishes. Fig. 8c) shows a case for

$$\theta = \theta_0 + \theta_1 \quad \text{with} \quad \theta_1 = \frac{1}{Lh} \int_{y-L_\beta}^{y+L_\beta} \int_{-h}^0 \mathcal{F}_u dz dy \quad \text{and}$$

$$\theta_0 = \frac{1}{L} \int_0^L (\mathcal{F}_u - \theta_1) dy \quad (15)$$

with $L_\beta = 500 \text{ km}$ and $\mathcal{F}_u = K_z f^2 N^{-2} \bar{u}_z$. In Eq. (15), the global momentum constraint is always satisfied by the constant gauge θ_0 and the close local correspondence of the parameterisation for \bar{s} with diffusion of potential vorticity is accomplished by θ_1 . Note that the meridional variations in θ_1 are small, i.e. of second order in quasi-geostrophic scaling, such that within that limit the diffusion of potential vorticity is unaffected. This means that with respect to the dynamics of the meso-scale eddies, the closure is still based on mixing of potential vorticity. However, allowing for the small meridional variation in θ , there is no exact correspondence with diffusion of planetary-geostrophic potential vorticity anymore. On the other hand, using Eq. (15) the strong meridional shear in the barotropic component of \bar{u} is eliminated, which is regarded as essential here because it has not been observed in the eddying models.

4.2.4. Prescribed K from the eddying model

Fig. 9 shows the zonal mean flow and mean isopycnals in the zonally averaged model using the diagnosed diffusivity K from the eddying model versions (Fig. 5) for the same combinations of L_r and σ as in Fig. 2. Note that the only modification of the diagnosed K from Fig. 5 is that in regions in which the diagnosed K was negative, the K used in the zonally averaged model was set to zero. The gauge term θ is chosen as in Eq. (15) with $\mathcal{F}_u = K(\bar{u}_{yy} - \beta) - K_z f^2 N^{-2} \bar{u}_z$ and $L_\beta = 300 \text{ km}$. The structure of the zonal jets is well reproduced by the closure in all cases, although the magnitude of the barotropic flow tend to be slightly underestimated. In the cases with largest

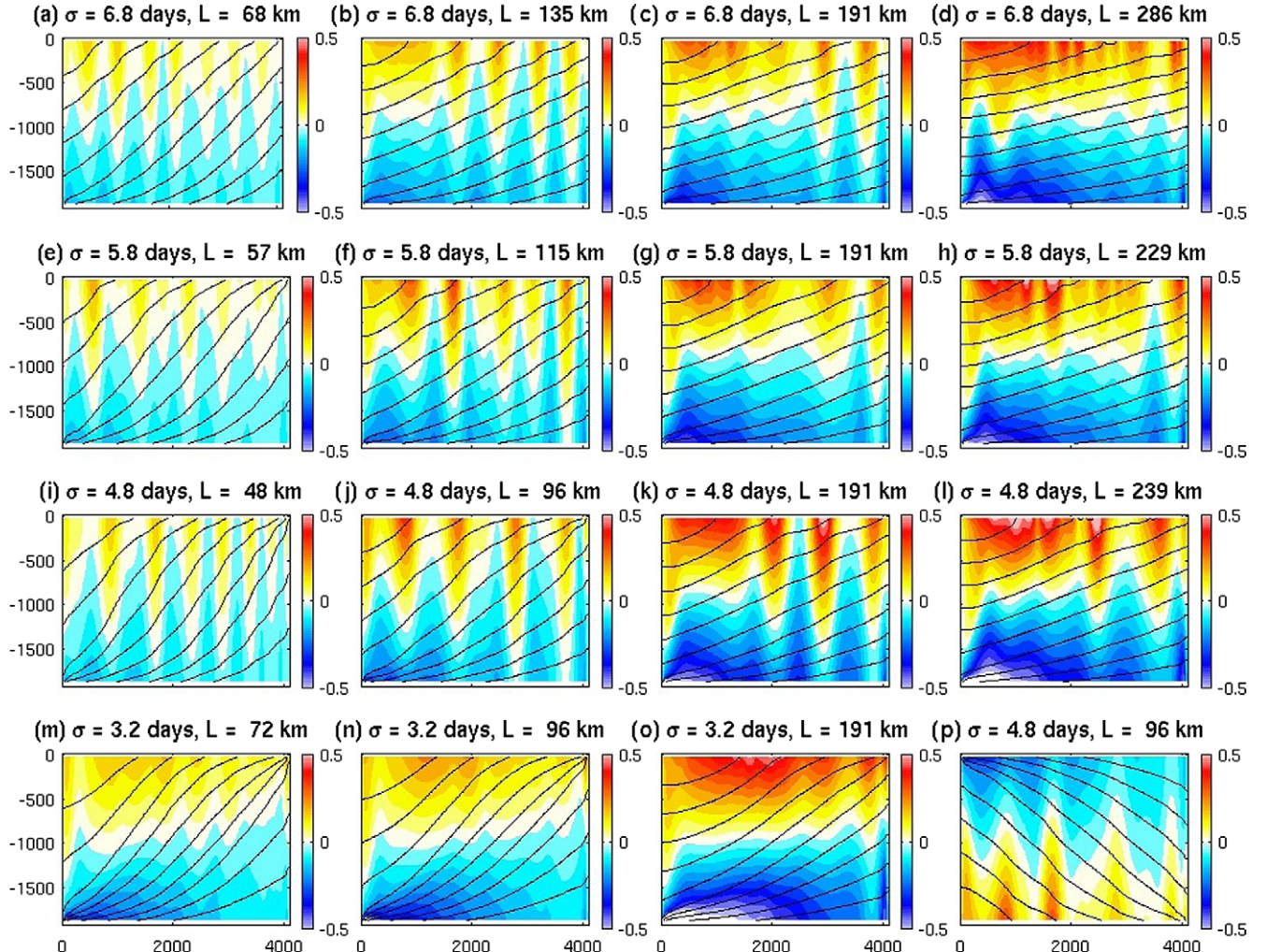


Fig. 9. Zonal mean zonal velocity in m/s in the zonally averaged model using K from the eddying version. Also shown are mean isopycnals (solid lines). The basin-wide Eady growth rate σ and Rossby radius L taken from Table 1 for the corresponding experiments are indicated in the figures.

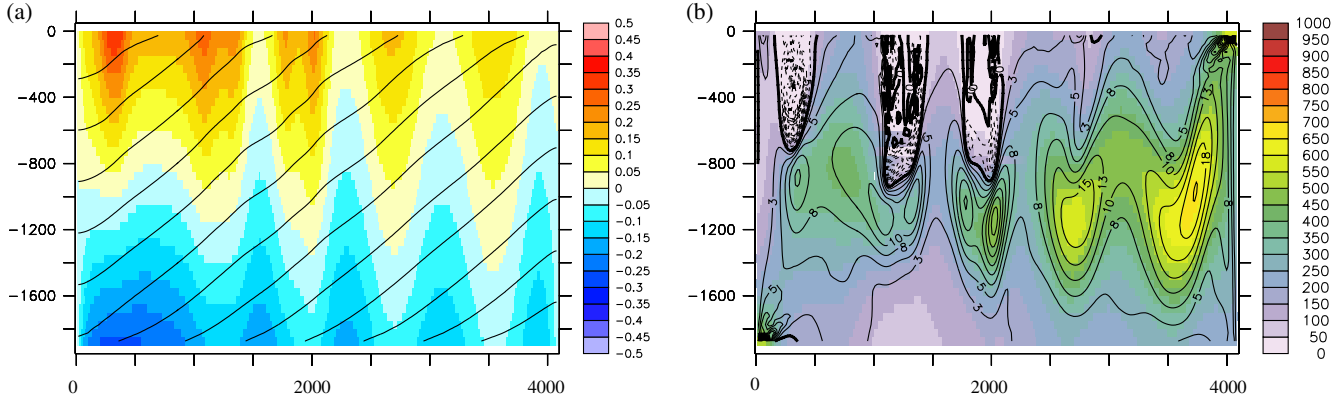


Fig. 10. (a) Zonal mean zonal flow in m/s in the coarse resolution model with EKE parameterisation and fixed length scale of 10 km after 600 days of simulation and for $L_r = 96$ km and $\sigma = 4.8$ d. (b) Parameterised EKE in cm^2/s^2 and parameterised EKE production terms in $10^{-9} \text{ m}^2/\text{s}^3$.

Rossby radii $L_r > 200$ km (cases d,h,l), however, small scale, near surface jets show up, which are not seen in the eddying model versions. These small-scale jets are related to the regions in which negative diffusivities in the uppermost model level have been diagnosed, which have been set to zero in the zonally averaged model versions. The same model misfit can be observed near the lateral boundaries where small regions with negative diffusivities show up in some of the eddying cases.

However, note that the local structure of the mean isopycnals is also well reproduced by the closure. Furthermore, it is important to note that without gauge term, i.e. violating the global momentum constraint, the zonally averaged model produces unrealistic zonal flow (not shown). The good agreement between the parameterised model and the eddying versions in all configurations is taken as evidence that the assumption of identical diffusivities for buoyancy and potential vorticity and the method to satisfy the global momentum constraint is valid.

4.2.5. Flow interactive K from a meso-scale eddy closure

In this section, the application of the meso-scale closure of Eden and Greatbatch (2008b) for K , as detailed in Appendix A, is discussed. The EKE budget given by

$$\bar{e}_t + v^* \bar{e}_y + w^* \bar{e}_z = KN^{-2} |\bar{b}_y|^2 - \bar{u}(K(\bar{u}_{yy} - \beta) + K_z f N^{-2} \bar{b}_y^* - \bar{\theta}) - 2r\bar{e} + (K\bar{e}_y)_y + (K_v \bar{e}_z)_z \quad (16)$$

is integrated as an additional model variable in the zonally averaged model using Eq. (12). The diffusivity $K = \bar{e}^{1/2} L$ is calculated using the EKE \bar{e} from Eq. (16) and a fixed eddy length scale L . Following Eden and Greatbatch (2008b), the radiative terms in the EKE budget, Eq. (16), have been parameterised as diffusion of EKE, with a lateral diffusivity K and a fixed vertical diffusivity of $K_v = 0.01 \text{ m}^2/\text{s}$. The length scale $L = 10 \text{ km}$ is taken to be constant for simplicity and the gauge term θ is chosen as in Eq. (15) with $\mathcal{F}_u = K(\bar{u}_{yy} - \beta) - K_z f^2 N^{-2} \bar{u}_z$ and $L_\beta = 300 \text{ km}$. Note that setting $\theta_1 = 0$, the basin-wide meridional shears of the barotropic zonal mean flow show up in the model experiments, which are not met in the eddying experiments and appear therefore undesirable.

Fig. 10 shows the mean zonal flow, EKE and EKE production terms in a simulation with $L_r = 96 \text{ km}$ and $\sigma = 4.8 \text{ d}$. Results are indeed similar to the eddying channel, however not identical. Eastward and surface intensified zonal jets are formed, which are forced by horizontal variations in K , i.e. local minima of K correspond to eastward jets, which is consistent with the eddying channel models. Other combinations of L_r and σ in the zonally averaged model cause similar variations of the mean zonal flow as in the eddying model (when tuning the eddy length scale as suggested

by the eddying model results). The parameterisation also simulates bottom intensified eastward jets when reversing the meridional buoyancy gradient M^2 . Moreover, the parameterised model show time dependency in some cases, i.e. zonal jets show up and merge together on a time scale of several years.

On the other hand, it is obvious that the parameterised EKE does not fit well the eddying models: Since the length scale L is constant, the EKE has a minimum in the jets in order to produce a minimum in K , which is inconsistent with the eddying channel, in which EKE is maximal within the eastward jets. This feature of the eddying model can thus not be reproduced, indicating a failure of the mixing length hypothesis with a fixed length scale. Note that choosing the local Rossby radius or Rhines scale (or the minimum between both), as suggested by Eden and Greatbatch (2008b), does not resolve the problem. It is stressed that this artifact of the closure could only be resolved when allowing for a spatially varying length scale with pronounced minima within the jets.

However, the EKE production terms are rather well parameterised, i.e. there is large baroclinic instability below the jets and barotropic instability in the cores of the jets feeding the mean flow, similar to the eddying channel. The most important production terms in the EKE budgets are the baroclinic production term $KN^{-2} |\bar{b}_y|^2$ and the barotropic production term $K_z f^2 N^{-2} \bar{u}_z$. The former is always positive and larger below the cores of the jets which was also observed for the eddying models (Fig. 3). K has a subsurface maximum within the cores of the eastward jets and, since \bar{u}_z is always positive, the term $-K_z f^2 N^{-2} \bar{u}_z$ is positive above the EKE maximum, i.e. forcing the eastward jets, and negative below.

5. Summary and discussion

5.1. Zonal jets in the eddying model

A suite of idealised channel models was analysed with respect to the validity of a closure for eddy momentum fluxes. Over a wide range of parameters, the eddying channel model exhibits surface intensified eastward zonal jets, a well-known feature of geophysical turbulence (Rhines, 1975). Note that such zonal jets can be found in all ocean basins (Treguier et al., 2003; Nakano and Hasumi, 2005; Maximenko et al., 2005; Eden, 2006) and the Southern Ocean, and that it is assumed that similar jet-like structures on giant gas planets like Jupiter and the atmospheric jet stream are governed by similar dynamical mechanism (Danilov and Gurarie, 2002; Galperin et al., 2004; Baldwin et al., 2007). Note also that these jets might play an important role in ventilating the interior mid-latitude ocean basins below the thermocline (Treguier et al.,

2003; Eden, 2006), such that a parameterisation of those features is necessary for ocean climate models predicting carbon uptake and other changes in biogeochemical cycles.

In the present eddying ocean model, the jets are formed by the lateral convergence of turbulent eddy momentum fluxes, i.e. they are eddy-driven – implying negative lateral eddy viscosities (Starr, 1968) – and they act as barriers for meridional turbulent exchange of buoyancy, potential vorticity and passive tracer (Dritschel and McIntyre, 2008) with reduced lateral diffusivities (Haynes et al., 2007). Accordingly, lateral diffusivities diagnosed from flux-gradient relations for eddy buoyancy and potential vorticity fluxes in the present model show pronounced minima within the eastward jets and maxima in the westward flow between (and below) the jets. Note that the relation between meridional variations (minima) of the lateral eddy diffusivity and the location of eddy-driven eastward zonal jets is also found in quasi-geostrophic channel models (Ivchenko et al., 1997; Olbers et al., 2000), which implies the possibility to implement the “negative viscosity effect” by downgradient potential vorticity mixing with a special lateral profile of the diffusivity. The vertical structure of the diffusivities features in all cases a strong gradient with largest values near the depth level at which the first baroclinic Rossby wave speed Doppler shifted by the mean flow cancels, i.e. to the steering level of unstable Rossby waves, where mixing is believed to be most intense (Green, 1970; Smith and Marshall, 2009). It was the aim of this study to parameterise the effects of the meso-scale fluctuations forming the eastward jets in a zonally averaged model, as a first step towards the application of an appropriate closure in a three-dimensional and more realistic context.

5.2. Diffusivity for buoyancy vs. potential vorticity

Welander (1973) first proposed to parameterise the effect of eddy momentum fluxes in ocean models by considering diffusion of potential vorticity, instead of momentum as in the micro-scale analogy, which implies negative viscosities within eddy-driven jets. However, this idea is hampered by the fact that potential vorticity is not a directly predicted variable in an ocean model based on the primitive equations. As one consequence, care has to be taken in the momentum budget, such that no forces are introduced by the parameterisation which would lead to spurious integral acceleration (Marshall, 1981). This goal was implemented by Wardle and Marshall (2000) and Olbers et al. (2000) by tuning the vertical structure of the diffusivity for the closure while prescribing magnitude and lateral shape of the diffusivity. In this study, on the other hand, a rotational flux of potential vorticity is introduced to satisfy the constraint on the momentum budget – given by the constant gauge term θ – in order to have freedom to choose the diffusivity, which can then be given for instance by a simple closure based on the mixing length assumption of Green (1970).

In order to keep the closure for the eddy momentum fluxes as simple as possible, it is assumed that the lateral diffusivity for buoyancy (i.e. the isopycnal thickness diffusivity) is identical to the one for potential vorticity. Since that diffusivity might be fixed, by for instance the mixing length assumption of Green (1970), a rotational eddy potential vorticity flux – given by the constant gauge θ in the present study – has to be introduced in order to satisfy the constraint on the momentum budget, when relating eddy potential vorticity fluxes with eddy momentum and buoyancy fluxes. In other words, the specification of the gauge term is used to insure that no spurious forces are introduced by the closure in the zonal momentum budget of the parameterised model. Since the gauge term drops out in the mean potential vorticity budget when taking the divergence of the eddy potential vorticity flux, it plays the role of a rotational flux component. While in Wardle

and Marshall (2000) and Olbers et al. (2000) the momentum constraint is satisfied by the choice of the prescribed value and vertical structure for K (while the gauge term is set to zero), in this study it is satisfied by the choice of the gauge term.

In the present study, diffusivities appropriate for eddy buoyancy and potential vorticity fluxes are diagnosed from flux-gradient relationships in the eddying channel model for a wide range of parameters. Although both diffusivities feature large lateral and vertical inhomogeneities, which also differ amongst the individual experiments a lot, the assumption of similar diffusivities for eddy buoyancy and potential vorticity fluxes is found to be valid in all channel experiments. Moreover, prescribing diffusivities from the eddying experiments in a zonally averaged model – with similar numerical discretisation and subgrid-scale dissipation as the eddying channel model and assuming identical diffusivities for buoyancy and potential vorticity – reproduces the zonal jets structure and small scale buoyancy variations rather well. Therefore, it is concluded here that the assumption of identical diffusivities for buoyancy and potential vorticity in a simple closure appears valid.

On the other hand, it is obvious from the diagnosis of the eddying channel models, that there are also differences between the diffusivities appropriate for buoyancy and potential vorticity. Those differences are large near the surface and also at the steering level at mid-depth, where the meridional gradient of the mean potential vorticity features a zero crossing such that the diffusivity appropriate for potential vorticity diagnosed from the flux-gradient relationship becomes ill-defined (Smith and Marshall, 2009). The differences can be related to regions in which isopycnals and isolines of mean potential vorticity are rather different. In those regions, one would expect a large impact of along-isopycnal diffusion, which is felt by tracers having gradients on mean isopycnals, but not by the mean buoyancy which is only affected by the thickness diffusivity and related bolus velocity (Eden and Greatbatch, 2009). In other words, potential vorticity is mixed also by isopycnal diffusion and is not just advected by the bolus velocity like buoyancy, which explains the differences in the diagnosed diffusivities in the eddying models. However, it appears that it is possible to ignore the complication of the impact of isopycnal diffusion on potential vorticity for a simple closure, since the zonally averaged model reproduces the results of the eddying model under this assumption rather well.

5.3. Zonal jets in the closure

The closure for the eddy momentum fluxes was tested using prescribed lateral diffusivities K in the zonally averaged model. A constant value for K does not reproduce the observed jet structure. In fact, it is found that horizontal variations in K lead to the zonal jets, i.e. meridional minima in K are related to eastward barotropic jets, which can be explained by the compensation between forces related to relative, planetary vorticity gradients and the gauge term, arising due to the implementation of potential vorticity mixing and the gauge term. The appearance of zonal jets – acting as mixing barriers with strongly reduced lateral diffusivities (Dritschel and McIntyre, 2008) – are therefore linked in the closure in a natural way and it appears possible to parameterise the appearance of zonal jets and its effect on the ventilation of interior ocean basins by implementation of potential mixing and the gauge term in realistic ocean model.

The application of the closure of Eden and Greatbatch (2008b) for K in the zonally averaged model, together with the choice for the gauge term and the specification of a constant eddy length scale yields the spontaneous generation of eastward zonal jets. The closure is given by a prognostic EKE budget with parameterised energy transfer terms related to baroclinic and barotropic instability and a fixed eddy length scale. The latter was chosen cor-

responding to integral length scales estimated from the eddying model. On the other hand, the fixed length scale is related to a drawback of the closure: since within the eastward zonal jets the diffusivity K has to have a local minimum, the mixing length assumption with a fixed length scale forces the EKE to have a local minimum in the jets. The eddying models, however, exhibit a local maximum of EKE within the jets, but a local minimum in the length scale. Therefore, the corrected simulation of EKE would only be possible if one would be able to model the lateral variations in the eddy length scale, for instance by adding another model equation.

On the other hand, the specific choice of the closure for K in principle does not affect the eddy momentum closure and the appearance of zonal jets by implementing potential vorticity mixing and the gauge term as discussed here. That is, for any closure of K which produces a minimum of K at some location (or for a prescribed K showing a minimum at that location) the implementation of potential vorticity mixing and the gauge term will produce a zonal jet at that location.

It should also be noted that the EKE-based closure of [Eden and Greatbatch \(2008b\)](#) automatically statisfies the “second constraint” of [Ivchenko et al. \(1997\)](#) on a parameterisation based on potential vorticity mixing. This constraint states that the existence of a nontrivial eddy regime requires positive production of EKE and EPE. This production is in quasi-geostrophic approximation proportional to the domain averaged product of the mean zonal velocity and the (parameterised) eddy potential vorticity flux. However, in the closure of [Eden and Greatbatch \(2008b\)](#), EKE and EPE production terms are parameterised such that a non-zero diffusivity shows up only when there is net production of eddy energy. Note that these parameterisations of the energy transfer terms are based on the same closures as for eddy buoyancy, potential vorticity and momentum fluxes. In that sense, the second constraint is build in that closure, while for a prescribed diffusivity, as discussed above, this is not the case.

5.4. Deviations from potential vorticity mixing

Prescribing vertical variations in K in the zonally averaged model reveals a complication of the proposed closure: Due to the large-scale changes of the Coriolis parameter in the primitive equation model, the implementation of potential vorticity mixing in the momentum equation generates large-scale meridional shear of the barotropic velocity which would not be present in quasi-geostrophic approximation. Such barotropic shear is not observed in the eddying models. By allowing for a small meridional dependency in the gauge term the undesired barotropic shear is eliminated. The close local correspondence of the eddy momentum flux parameterisation with diffusion of quasi-geostrophic potential vorticity is guaranteed since the meridional dependency of the gauge term is negligible in quasi-geostrophic scaling. In effect, the principle of potential vorticity mixing by meso-scale fluctuations was localised with respect to a lateral extent over which the quasi-geostrophic approximation remains valid. On the other hand, there is no exact correspondence with diffusion of planetary-geostrophic potential vorticity anymore.

A further complication of the closure is given by rotational fluxes of potential vorticity across the lateral boundaries: Since the same diffusivity is used for the eddy buoyancy and potential vorticity fluxes, setting the diffusivity to zero at the lateral boundary only satisfies vanishing eddy buoyancy fluxes across boundaries, while there is still a cross-boundary rotational eddy potential vorticity flux given by the gauge term θ . A simple solution to this problem would be to deviate from the principle idea of potential vorticity mixing at the boundary by setting θ to zero at the boundaries, while still satisfying the global momentum constraint

by the choice of θ in the interior. Note that in the zonally averaged model, there is not much difference in the solutions by doing so (not shown) such that it might be possible to simply ignore that problem. However, note also that it is guaranteed in any case that no spurious integral forces are introduced by the closure since the integral momentum constraint is always satisfied by the appropriate choice of θ . Furthermore, by introducing the localised momentum constraint, spurious forces are also locally suppressed.

Acknowledgments

This study was supported by the German DFG as part of the SPP 1158 and the SFB 754. Suggestions and discussions with Dirk Olbers and Richard Greatbatch and suggestions by two anonymous reviewers have been helpful and are appreciated.

Appendix A. The closure of [Eden and Greatbatch \(2008b\)](#)

The mixing length hypothesis for geostrophic turbulent flow of [Green \(1970\)](#) for the eddy buoyancy flux was adopted by [Eden and Greatbatch \(2008b\)](#), i.e. it was assumed that the eddy buoyancy flux is directed down the mean gradient, Eq. (6), with a lateral diffusivity $K = \bar{e}^{1/2}L$, where \bar{e} denotes EKE and L an appropriate eddy length scale. Introducing \bar{e} as an additional variable in a non-eddy-resolving model, using a prognostic budget for EKE with parameterised sources and sinks and a diagnostic relation for L yields the lateral diffusivity K in the simple closure.

[Eden and Greatbatch \(2008b\)](#) assumed that in the EPE balance, Eq. (23), production of EPE (by $N^2\bar{h}\bar{b}_y$) balances transfer to EKE (by $N^2\bar{b}'w'$). This assumption is related to small or vanishing diapycnal mixing due to meso-scale eddies ([Eden and Greatbatch, 2008a](#)). It follows that

$$-\bar{h}\bar{b}_y \approx K\bar{b}_y^2 \approx \bar{b}'w' \quad (17)$$

Using the closure Eq. (17) in the EKE budget Eq. (21) yields

$$\bar{e}_t = KN^2\bar{b}_y^2 - \bar{s}\bar{u}_y - 2r\bar{e} - (\bar{v}'\bar{p}')_y - (\bar{w}'\bar{p}')_z - (\bar{v}'\bar{e})_y \quad (18)$$

[Eden and Greatbatch \(2008b\)](#) suggested to parameterise the non-local radiative and advective terms, i.e. $-(\bar{v}'\bar{p}')_y - (\bar{w}'\bar{p}')_z - (\bar{v}'\bar{e})_y$ in Eq. (18), as diffusion of EKE. With an appropriate parameterisation for the energy exchange term with MKE, $\bar{s}\bar{u}_y$ in Eq. (18), the parameterised EKE budget can then be used to predict \bar{e} in a zonally averaged model. Specifying a diagnostic eddy length scale L yields then K and a closure for the eddy buoyancy flux \bar{h} .

Using expression Eq. (8) (with $K = K'$) for \bar{s}_y in the MKE budget, Eq. (22) yields

$$m_t = \bar{b}\bar{w} + \bar{S} - (\bar{p}\bar{w})_z - 2rm \quad \text{with} \quad \bar{S} = u(K(\bar{u}_{yy} - \beta) + K_z f \bar{b}_y - \bar{\theta}) \quad (19)$$

The term \bar{S} in the parameterised MKE budget, Eq. (19), can be identified as the parameterised exchange of MKE with EKE and \bar{S} can now be inserted in the EKE budget (with opposite sign) as a parameterisation for this energy exchange. However, note that in order to derive Eq. (19), in the original MKE budget, Eq. (22), both terms related to the eddy momentum fluxes $(\bar{s}\bar{u}_y - (\bar{s}\bar{u})_y)\bar{u}_y$ have been combined to yield the exchange term \bar{S} in Eq. (19). On the other hand, the sum of the terms related to the eddy momentum fluxes in the MKE budget Eq. (22) is not exactly what can be found as exchange term in the EKE budget, Eq. (21), i.e. only $\bar{s}\bar{u}_y$ shows up in the EKE budget, while the advective term in the MKE budget, $(\bar{u}\bar{s})_y$, is missing in the EKE budget. Only in the basin integrated form of the Lorenz energy cycle, where the advective term in the MKE budget cancels, there is a closed energy exchange between MKE and EKE.

The complication given by the mismatch of the energy exchange terms in the MKE and EKE budgets was ignored by [Eden and Greatbatch \(2008b\)](#) and the energy exchange term $\bar{s}u_y$ in the EKE budget is simply replaced by \bar{S} . The parameterised EKE budget finally becomes

$$\bar{e}_t = KN^2\bar{b}_y^2 - \bar{S} - 2r\bar{e} - (\bar{v}'(p' + e))_y - (\bar{w}'p')_z \quad (20)$$

The remaining advective and radiative terms in Eq. (20) are parameterised as diffusion of EKE which then leads to Eq. (16) (in which also advection of \bar{e} by the residual flow was included).

Appendix B. Energy cycle

The eddy kinetic energy (EKE, $\bar{e} = \frac{1}{2}\bar{u}_i^2$), the mean kinetic energy (MKE, $\bar{m} = \frac{1}{2}\bar{u}^2$) and the eddy potential energy (EPE, $\bar{\phi} = \frac{1}{2}N^2\bar{b}^2$) for the zonally averaged case are given by

$$\bar{e}_t + (\bar{v}'\bar{e})_y = N^2\bar{b}'\bar{w}' - \bar{s}\bar{u}_y - (\bar{v}'\bar{p}')_y - (\bar{w}'\bar{p}')_z - 2r\bar{e} \quad (21)$$

$$\bar{m}_t + (\bar{u}\bar{s})_y = N^2\bar{b}\bar{w} + \bar{s}\bar{u}_y - (\bar{p}\bar{w})_z - 2rm \quad (22)$$

$$\bar{\phi}_t + (\bar{v}'\bar{\phi})_y = -N^2\bar{b}'\bar{w}' - N^2\bar{h}\bar{b}_y + N^2\bar{b}'Q' \quad (23)$$

Together with the budget for the mean potential energy (MPE, $\frac{1}{2}N^2\bar{b}^2$), Eqs. (21)–(23) describe the energy cycle in the channel model, which is also sometimes called the Lorenz energy cycle ([Lorenz, 1955](#)). The terms in the budgets can be interpreted as storage, forcing, dissipation and energy exchange terms on the one hand and advective or radiative terms on the other hand. This differentiation is useful since the latter vanish in the integral over the domain. The term $\bar{s}\bar{u}_y$, showing up with opposite sign in the EKE budget, Eq. (21), and the MKE budget, Eq. (22), describes energy exchange from EKE to MKE due to horizontal shear of the mean flow and is often related to barotropic instability. The term $N^2\bar{b}'\bar{w}'$ in the EPE budget, Eq. (23), describes exchange from EPE to EKE and is often related with baroclinic instability.

References

- Andrews, D.G., Holton, J.R., Leovy, C.B., 1987. Middle Atmosphere Dynamics. Academic Press.
- Baldwin, M., Rhines, P., Huang, H., McIntyre, M., 2007. ATMOSPHERES: The jet-stream conundrum. *Science* 315 (5811), 467.
- Bretherton, F., 1966. Critical layer instability in baroclinic flows. *Quart. J. Royal Met. Soc.* 92, 325–334.
- Danilov, S., Gurarie, D., 2002. Rhines scale and spectra of the β -plane turbulence with bottom drag. *Phys. Rev. E*, 65.
- Dritschel, D.G., McIntyre, M.E., 2008. Multiple jets as PV staircases: The Phillips effect and the resilience of eddy-transport barriers. *J. Atmos. Sci.* 65 (3), 855–874.
- Eden, C., 2006. Mid-depth equatorial tracer tongues in a model of the Atlantic Ocean. *J. Geophys. Res.* 111 (C12025). doi:[10.1029/2006JC003565](https://doi.org/10.1029/2006JC003565).
- Eden, C., Greatbatch, R.J., 2008a. Diapycnal mixing by mesoscale eddies. *Ocean Model.* 23 (3–4), 113–120.
- Eden, C., Greatbatch, R.J., 2008b. Towards a mesoscale eddy closure. *Ocean Model.* 20, 223–239.
- Eden, C., Greatbatch, R.J., 2009. A diagnosis of isopycnal mixing by meso-scale eddies. *Ocean Model.* 27 (1–2), 98–106.
- Eden, C., Greatbatch, R.J., Olbers, D., 2007. Interpreting eddy fluxes. *J. Phys. Oceanogr.* 37, 1282–1296.
- Ferreira, D., Marshall, J., 2006. Formulation and implementation of a residual-mean ocean circulation model. *Ocean Model.* 13, 86–107.
- Galperin, B., Nakano, H., Huang, H.-P., Sukoriansky, S., 2004. The ubiquitous zonal jets in the atmospheres of giant planets and earth's oceans. *Geophys. Res. Lett.* 32 (L13303). doi:[10.1029/2004GL019691](https://doi.org/10.1029/2004GL019691).
- Gent, P.R., McWilliams, J.C., 1990. Isopycnal mixing in ocean circulation models. *J. Phys. Oceanogr.* 20, 150–155.
- Green, J.S., 1970. Transfer properties of the large-scale eddies and the general circulation of the atmosphere. *Quart. J. Royal Met. Soc.* 96, 157–185.
- Haynes, P., Poet, D., Shuckburgh, E., 2007. Transport and mixing in kinematic and dynamically consistent flows. *J. Atmospheric Sci.* 64 (10), 3640–3651.
- Ivchenko, V.O., Richards, K., Sinha, B., Wolff, J.O., 1997. Parameterization of mesoscale eddy-fluxes in zonal flow of the ocean. *J. Mar. Sys.* 55 (6), 1127–1162.
- Killworth, P.D., 1997. On the parameterization of eddy transfer. Part I. Theory. *J. Mar. Res.* 55, 1171–1197.
- Large, W., Danabasoglu, G., McWilliams, J., Gent, P., Bryan, F., 2001. Equatorial circulation of a global ocean climate model with anisotropic horizontal viscosity. *J. Phys. Oceanogr.* 31 (2).
- Lorenz, E.N., 1955. Available potential energy and the maintenance of the general circulation. *Tellus* 7, 157–167.
- Marshall, J.C., 1981. On the parameterization of geostrophic eddies in the ocean. *J. Phys. Oceanogr.* 11, 1257–1271.
- Maximenko, N.A., Bang, B., Sasaki, H., 2005. Observational evidence of alternating zonal jets in the world ocean. *Geophys. Res. Lett.* 32 (L12607). doi:[10.1029/2005GL022728](https://doi.org/10.1029/2005GL022728).
- McDougall, T.J., McIntosh, P.C., 1996. The temporal-residual-mean velocity. Part I: Derivation and the scalar conservation equation. *J. Phys. Oceanogr.* 26, 2653–2665.
- Nakano, H., Hasumi, H., 2005. A series of zonal jets embedded in the broad zonal flows in the Pacific obtained in eddy-permitting ocean general circulation models. *J. Phys. Oceanogr.* 35 (4), 474–488.
- Olbers, D., Wolff, J., Völler, C., 2000. Eddy fluxes and second-order moment balances for nonhomogeneous quasigeostrophic turbulence in wind-driven zonal flows. *J. Phys. Oceanogr.* 30 (7), 1645–1668.
- Plumb, R.A., Ferrari, R., 2005. Transformed eulerian-mean theory. Part I: Nonquasigeostrophic theory for eddies on a zonal-mean flow. *J. Phys. Oceanogr.* 35 (2), 165–174.
- Rhines, P., 1975. Waves and turbulence on a beta-plane. *J. Fluid Mech.* 69, 417–443.
- Smith, K., Marshall, J., 2009. Evidence for enhanced eddy mixing at middepth in the Southern Ocean. *J. Phys. Oceanogr.* 39 (1), 50–69.
- Starr, V.P., 1968. Physics of Negative Viscosity Phenomena. McGraw-Hill, New York, USA.
- Treguier, A.M., Held, I.M., Larichev, V.D., 1997. Parameterization of quasigeostrophic eddies in primitive equation ocean models. *J. Phys. Oceanogr.* 27, 567–580.
- Treguier, A.M., Hogg, N.C., Maltrud, M., Speer, K., Thierry, V., 2003. The origin of deep zonal flows in the Brazil Basin. *J. Phys. Oceanogr.* 33 (3), 580–599.
- Wardle, R., Marshall, J., 2000. Representation of eddies in primitive equation models by a PV flux. *J. Phys. Oceanogr.* 30, 2481–2503.
- Welander, P., 1973. Lateral friction in the oceans as an effect of potential vorticity mixing. *Geophys. Astrophys. Fluid Dyn.* 5 (1), 173–189.
- Zhao, R., Vallis, G., 2008. Parameterizing mesoscale eddies with residual and Eulerian schemes, and a comparison with eddy-permitting models. *Ocean Model.* 23 (1–2), 1–12.